JOURNAL OF OPTOELECTRONICS AND ADVANCED MATERIALS Vol. 8, No. 3, June 2006, p. 1194 - 1199

Nanomechanical properties evaluation of bioactive glass coatings on titanium alloy substrate

C. Y. TANG[a*], C. P. TSUI[a], DJ. JANACKOVIC[b], P. S. USKOKOVIC[b]
[a]*Department of Industrial and Systems Engineering, The Hong Kong Polytechnic Unversity, Hung Hom, Kowloon, Hong Kong, P.R. China*
[b]*Faculty of Technology and Metallurgy, University of Belgrade, Karnegijeva 4, 11000 Belgrade, Serbia and Montenegro*

Bioinert metallic implants such as titanium and titanium alloys could be coated with bioactive materials with good adhesion to metal and which could be also bonded to the bone. In order to predict the mechanical behavior of coatings during the implant insertion, mechanical properties of the surface and through the thickness of deposited bioglass coatings are necessary to be studied. We report an investigation of the mechanical characteristics of bioglass coatings using the nanoindentation and nanoscratch techniques. The coating topography with residual imprints was analyzed by *in situ* imaging method. The dependence of the friction coefficient on load in constant and ramped load tests as well as on the scratch speed is compared. Elastic modulus and hardness results after indentation on the coating surface with higher loads showed more consistent results with less pile up around imprints. The nanohardness and reduced elastic modulus of the coating is in the expected boundaries of theoretical values for glass and alloy with a moderate distribution through the coating thickness. Nanoscratch testing showed that the surface deform plastically with no visible debris or cracks.

(Received February 12, 2006; in revised form May 4; accepted May 18, 2006)

Keywords: Bioglass coating, Nanoindentation, Nanoscratch

1. Introduction

Metallic artificial implants are bioinert, which could lead to encapsulation by dense fibrous tissue in the body and unsuitable stress distributions at the bone-implant interface that can lead to interfacial failure. Therefore, metal implants could be coated with bioactive materials with good adhesion to metal and which could promote the formation of hydroxyapatite (HAp), the inorganic component of natural bone, and bonding to the bone tissue. Bioactive glasses based on mixtures of the oxides of silicon, sodium, potassium, calcium, and magnesium, have been obtained by enamelling technique deposition on the metal surface with subsequent annealing at 800-900 °C [1-3]. By adjusting the coating stoichiometry, the thermal expansion coefficient of the glass can be made to match that of the Ti alloy, avoiding the generation of thermal stresses at the interface. The softening point of these glasses is lower than the temperature of $\alpha \rightarrow \beta$ transformation of titanium. At the same time, glass coatings with silica contents lower than 60 wt.% has shown good in vitro behaviour in simulated body fluid (SBF) solution [1-4], and other with silica content higher than 60 wt.% had a better mechanical stability and adhesion to the substrate but are no longer bioactive.

Conventional indentation tests were used to qualitatively analyse the mechanical properties of the coating as well as observing crack propagation and fracture surfaces in the vicinity of the interface [4]. As opposed to conventional indentation, nanoindentation method can give directly the elastic modulus and nanohardness of the areas of interest after materials processing and has attracted an increasing attention in the biomaterial [5,6] and surface and coating science [7,8]. Nanoindentation and nanoscratch studies were reported on HAp thin films deposited on Ti alloy substrates [9-12]. During the insertion process of the implant part into the bone and in the period of usage before complete osseointegration, asperity interactions due to the very small nano-level hydroxyapatite (HAp) particles from natural bone as well the interaction with the body fluids and cell matrix may lead to damage of the implant or formation of wear debris. Therefore, bioactive glass coatings exhibiting wear resistance and predetermined surface mechanical properties are of great importance for high-load bearing implants. Diamond tip of small radius of curvature, attached to a force-displacement transducer capable of applying and sensing normal and tangential forces in a controlled fashion, could be used to estimate locally Young modulus and hardness and simulate sliding of an asperity on the coating surface. In order to predict the mechanical behavior of coatings during the implant insertion and to enlighten the feasibility of the nanomechanical methods, in this work, the mechanical properties of the surface and through the thickness of deposited bioglass coating were investigated using the nanoindentation and nanoscratch technique.

2. Experimental

Bioactive glass was synthesized with the composition (wt. percent): 56.5% SiO_2, 15% CaO, 11% Na_2O, 8.5%

MgO, 6% P_2O_5 and 3% K_2O, with the coefficient of thermal expansion $\alpha = 10.2 \times 10^{-6}$ ºC^{-1}. The mixture was first dried and then fired in air for 80 min. in a Pt crucible firstly rising the temperature to 850 ºC. This temperature was kept for 60 min. followed by temperature rise to 1500 ºC for 65 min. (heating time rate 10 °C/min). This temperature was kept for 90 min. followed by rapid cooling in cold water.

To manufacture the coatings, the glass was pulverized in the planetary mill for 60 min. and sieved to the particle size below 40 μm. Glass powders 6P57 were dispersed in distilled water and submitted to ultrasonification for 15 min. in order to deagglomerate glass particles. Prepared dispersion was kept for 20 min. before pouring into spray bottle and depositing onto Ti_6Al_4V plates, which were previously polished and cleaned in acetone and ethanol. During spray deposition of glass particles, the Ti alloy substrate was held at 300 °C in order to enable evaporation of water. After completion of glass deposition, samples were thermally processed in vacuum furnace in order to sinter the coating. The specimens were heated to 550 ºC for 5 min. after which the furnace was air evacuated for 7 min. Subsequently, they were heated to 890 ºC, and once the desired temperature was reached it was held for 1 min. After that period, air was let into the chamber and the sample was taken out of the furnace and cooled in air. The surface of glass coating was not polished prior to testing, while the cross section of the plate was polished with diamond paste to an average roughness below 0.1 μm.

Nanoindentation and nanoscratch experiments were carried out using a Triboscope Nanomechanical Testing System (Hysitron Inc., Minneapolis, MN) equipped with *in situ* imaging mode, which offers the ability to provide images with the same probe tip that is used to perform the nanomechanical testing. During indentation, a diamond indenter was pushed into the surface of the sample while the load and displacement of the indenter are continuously monitored with resolutions of 0.1 μN and 0.2 nm, respectively. A Berkovich indenter was used, which is a three-sided pyramid with a total included angle of 142.3° and a tip radius of 150 nm. Loading/unloading rates for nanoindentation were set to 10 μN/s. By using a very light loading force (0-1 μN), the *in situ* imaging method can measure surface topography without causing any damage to the surface, just as the standard atomic force microscopy can do. Nanoscratch tests were accomplished by applying a normal load in a controlled manner while measuring the force required to move the tip laterally across the sample. By detecting the lateral force and normal displacement, the friction coefficient relative to the scratch depth was determined by the ratio of the lateral force to the normal force.

3. Results

3.1. Indentations on the coating surface

Fig. 1 shows SEM micrographs of the coating made by spraying the glass dispersion 6P57 on the Ti alloy and heating to 890 ºC. Micrograph shows absence of porosities and good wetting between coating and substrate during thermal treating due to the compatibility of the coefficients of thermal expansion. The average coating thickness was measured to be about 7 μN.

Characteristic loading–unloading curves for three loading values imposed on the bioglass surface are presented in Fig. 2. The unloading data are used to determine the mechanical properties based on the indentation theory, that the initial unloading portion of the load-depth curve represents purely elastic recovery. The slope of this unloading segment, S, is a measure of the material stiffness, referred to as the contact stiffness. From the load-depth curve, the elastic modulus and hardness are calculated based on the methods proposed by Oliver and Pharr [13]. The equations used are:

$$E_r = \frac{\sqrt{\pi} S}{2\sqrt{A}}$$

where A is the indenter contact area, and E_r, the reduced modulus, is defined by:

$$\frac{1}{E_r} = \frac{\left(1 - \nu_m{}^2\right)}{E_m} + \frac{\left(1 - \nu_i{}^2\right)}{E_i}$$

where E_m and ν_m are the Young's modulus and Poisson's ratio of the indented materials, respectively, and E_i and ν_i are those of the diamond indenter, given as $E_i = 1141$ GPa and $\nu_i = 0.07$. The material hardness, H, is defined as the maximum load, P_{max}, divided by the projected area of the indentation under this load, i.e., $H = P_{max}/A_{max}$.

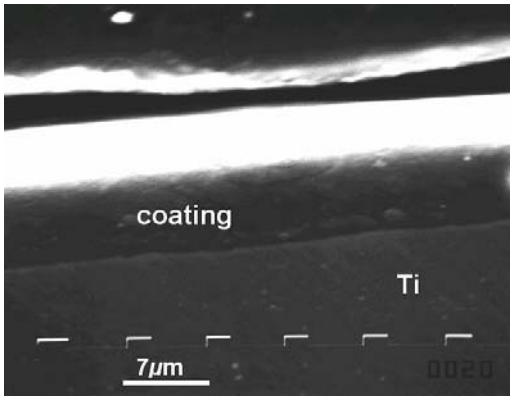

Fig. 1. SEM micrograph of the cross section angular view in the vicinity of the interface.

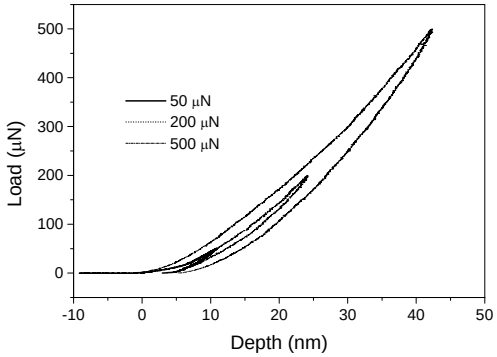

Fig. 2. Load-depth curves for coating surface under various loads.

3.2. Indentations on the cross section

Three rows of 8 indents with 3 loading values (1, 2 and 3 mN) each were placed on the cross section surface. Indents were placed with 2 μm between each one and rows were separated with 5 μm. Each row of indents on the cross-section surface spanned the 15 μm thickness of the sample to obtain the hardness and Young modulus through the sample starting from the alloy and finishing in the bioglass. Fig. 3 shows reduced modulus and hardness versus location for the cross section area. Fig. 4 shows the plot of a representative indentation mark on the cross section surface at 5 mN load.

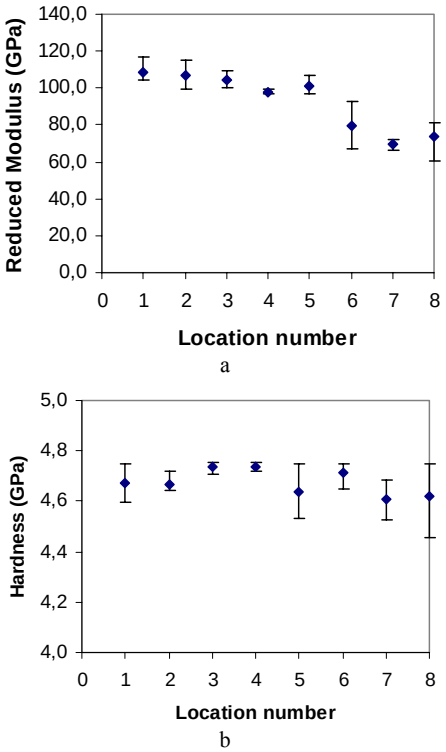

Fig. 3. (a) Reduced modulus versus position for the cross section area; (b) Hardness versus position for the cross section area. Locations 6 - 8 are made on the coating region. Indentation load was 1 mN.

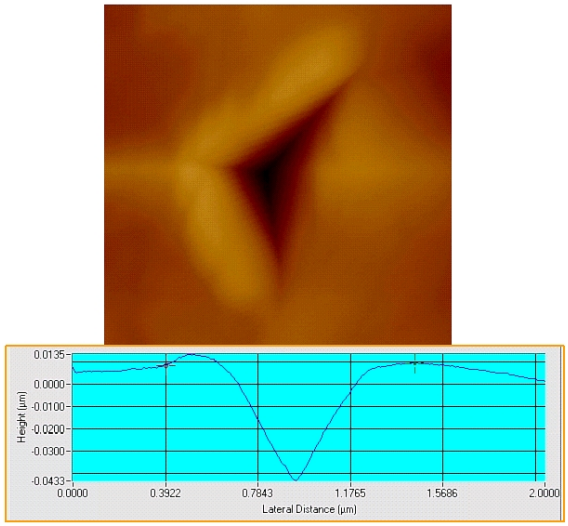

Fig. 4. Indent mark and surface profile at the cross section area of glass coating after 5 mN loading.

3.3. Nanoscratch testing

A Berkovich diamond tip was aligned to scratch the coating surface in a face-forward direction using three maximum loads (50, 200 and 500 μN) for the ramped tests and the same three loads for the constant load tests. A scratch length of 10 μm and a scratch rate of 0.33 μm/s were chosen for the experiment. Surface profiles before and after scratching were obtained by scanning the tip at 1 μN normal load, a load small enough that produced no measurable displacement. The friction coefficients were monitored around 2050 data points over the whole length of the scratch and the data from 20 to 40 s are used to calculate the average friction coefficient. It should be noted that the scratch time is 30 s but the overall recorded time cover the tip insertion, scratch and tip removal from the sample.

During the implant insertion process, it is expected that the coating surface will undergo scratching by HAp nanoparticles from the surrounding bone tissue. After scratching with Berkovich tip, formation of cracks and debris was examined by using in situ imaging method.

Fig. 5 (a) – (c) shows representative friction coefficient traces obtained by sliding a tip on the coating surface under different scratch regimes. Residual imprints of scratch grooves under ramp scratch load can be observed in Fig. 5 (d). The scan was taken at the end of a scratch trace. Fig. 6 (a) shows coefficient of friction for various sliding speed and a contact force equal to 200 μN constant load. Average values for the coefficient of friction, which are taken from 15-25 s period are presented in Fig. 6 (b).

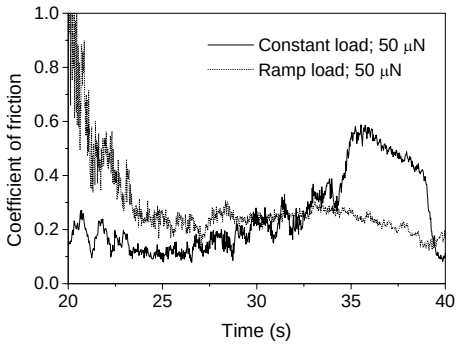

a

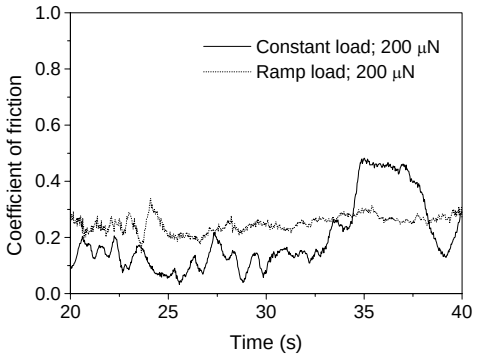

b

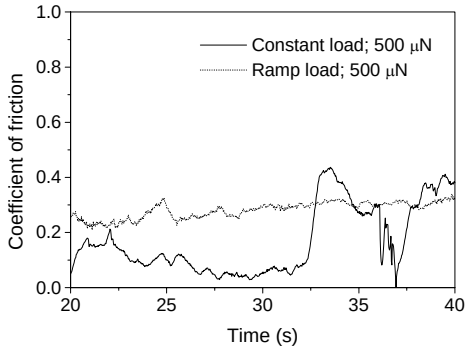

c

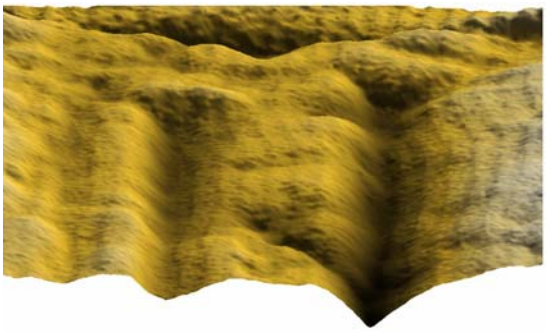

d

Fig. 5. (a) – (c) Coefficient of friction values for various constant and ramp loads; (d) Residual imprints of scratch grooves under ramp scratch load.

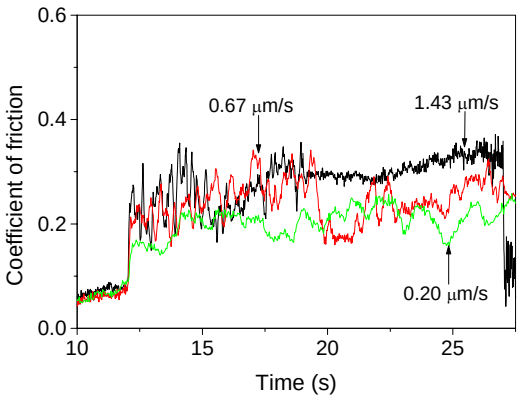

a

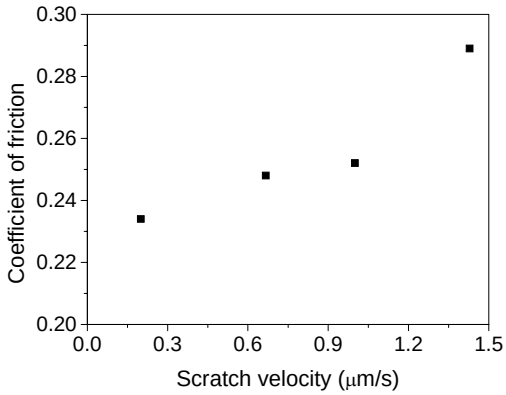

b

Fig. 6. (a) Coefficient of friction traces for various scratch velocities; (b) Average coefficient of friction vs. scratch velocity.

4. Discussion

4.1. Indentations on the coating surface

Overall results of nanoindentation tests are presented in Table 1, with the average values calculated from at least 5 indents. Indentations with the laod-unload curves, which show pop-up or other irregularities are excluded from calculations. The average reduced modulus is reasonably comparable to the reported values from macroscopic tensile tests of 6P57 glass (80-90 GPa [14]). Unlike modulus, which doesn't show regular trend behaviour regarding to the applied load, hardness increased with higher applied load. This is probably due to measurement errors at the small indentation depth, which is about 10 nm. The tip radius is more than ten times bigger than the indentation depth and the deformation volume of the material beneath the tip is so small; that generates measurement uncertainty. In the study by Teghil et al. [15], hardness decrease in the topmost layers is explained by the hydration at the surface layers of the bioglass. Mean

surface roughness, R_a, by *in situ* imaging for all samples is shown to be less than 0.1 μm without additional polishing of the surface.

Table 1. Reduced modulus and hardness of coating surface for two load levels; standard deviations (S.D.) are shown in brackets.

Load (μN)	E_r (GPa)	H (GPa)
50	90.355 (4.459)	3.246 (0.592)
200	80.904 (4.311)	5.729 (1.456)
500	83.733 (0.887)	7.848 (1.014)

4.2. Indentations on the cross section

From Fig. 3 it can be observed that results for the bioglass elastic modulus distribution agree well and fall within the range reported in the literature for 6P57 glass and Ti6Al4V alloy [14,16-18]. Because the spacing between indentations are nearly equal, the reduced modulus and the nanohardness show a distribution through the thickness with the values falling between glass and Ti alloy. However, there is a slight spread in the reported values, which could be attributed to the surface roughness. This moderate distribution could be beneficial to the structure materials for dissipation or decreasing the stress concentration that could appear at the interfaces. Distinct interface glass/alloy cannot be observed by in situ imaging and conventional nanoindentation, because the mechanical properties of two phases are similar. None of our measurements suggested that properties increased from the surface side to the boundary side in a descriptive manner, so caution must be used in interpreting these results.

For all imposed loads, triangular indents are clearly observed with depths varying with applied loads. From in situ imaging scans, no visible cracks were found around the indent (1, 2, 3 and 5 mN). At higher indentation loads (5 mN), there was slight material pile-up (Fig. 4).

4.3. Nanoscratch testing

As shown in Fig. 5(a), significant fluctuations (S.D. is 0.144) of the friction coefficient for constant load were observed at light contact loads due to the high sensitivity of the force transducer to the noise induced by the surface roughness. Surface imaging of the tested surface with lowest load did not yield apparent evidence of permanent deformation, suggesting that deformation of glass surface was mainly elastic. Thus, the magnitudes of the measured friction coefficients can be attributed to surface adhesion and surface roughness effects.

The friction coefficient measurements presented in Fig. 5 (a)-(c) are also revealing more steady-state sliding conditions for ramped load tests in comparison to constant load conditions. Small deviations from this behaviour are observed at the very beginning and the end of the scratches and these are associated with application and release of the load. For lowest applied load, ramp load exhibit fluctuations, while for higher loads, friction coefficient traces are rather steady. In a scratch test, the cracking of a coating is signalled by a sudden increase in coefficient of friction. The load associated with this event is called the "critical load". Results indicate that constant contact loads as high as 50 μN are above the critical load for glass coating. Conversely, for ramped contact loads there is no evidence of cracking, which could indicate that measured values for coefficient of friction are more reliable.

Intense friction coefficient variations are often associated with rapid changes of the real contact area due to the formation and entrapment of debris at the contact interface. By observing in situ imaging scan of the last ~2 μm length of the scratch residual imprint (i.e. at load value approximately equal to the fixed load scratches, Fig. 5 (d)), there is no evidence of bursts in the friction trace or debris, which is in agreement with steady trend of friction coefficient traces for ramped loading regime. It is also important to note that for constant load scratching we found sporadic formation of peaks in residual tracks and higher roughness of scratch tracks in comparison to ramped load regime. No clearly observable cracks were initiated in glass coating up to the 500 μN ramp scratch load (Fig. 5 (d)).

Table 2 shows the average coefficient of friction as a function of load during ramped and constant scratches. With the increase of constant load, the coefficient of friction decreases. The rate of decrease declines with load. It is likely that coefficient of friction is more influenced by the nanoscale surface topography in the low load regime than at higher loads. Under the same load (maximum), the ramp load tests exhibit slightly, but steadily, higher coefficient of friction. By comparing the results from glass surface indentation and scratch tests, it can be observed that by increasing the indentation and scratch (in ramped load regime) loads, hardness and friction coefficient increases. The layer near the surface with lower hardness serves to provide low friction performance, and the base layer with higher hardness serves to reduce mechanical property differences at the interface, thereby exhibiting a high friction coefficient and enhancing adhesive strength between the coating and substrate.

Table 2. Coefficients of friction for constant and ramped scratch loads in dependence of contanct load; (S.D.) are shown in brackets.

Load (μN)	Coefficient of friction	
	Constant load	Ramp load
50	0.255 (0.144)	0.232 (0.037)
200	0.196 (0.124)	0.250 (0.028)
500	0.170 (0.124)	0.281 (0.029)

Average values for the coefficient of friction presented in Fig. 6 (b), are in the range of 0.209 – 0.285 and show a trend to increase with increasing sliding speed. For elastic contacts, the coefficient of friction is mainly due to surface adhesion, which is independent of sliding speed [19]. Plastic deformation by the relatively sharp diamond tip has occurred under the aforementioned

contact conditions, which is confirmed by the formation of scratches on the glass surface. Thus, the increase of the friction coefficient with sliding speed may be attributed to strain rate effects.

5. Conclusions

The first direct investigation to our knowledge of the nanomechanical properties of bioactive glass coating on Ti-alloy by nanoindentation and nanoscratch is presented in order to elucidate surface mechanical behavior of the implant, which is especially important during insertion process. Significant nanohardness differences were observed between surface indents under different loads. The nanohardness and reduced modulus of the coating are in the expected boundaries of theoretical values for glass and Ti alloy with a moderate distribution through the coating thickness. For constant load, the general trend was for the coefficient of friction to decrease with increasing contact load. For ramped load, coefficient of friction traces were found to be steadier and the average values were increasing with increasing the contact load. The tendency was for the coefficient of friction to increase at higher sliding speeds, most likely due to strain rate effects. In general, the scratch surfaces on the glass coating indicate certain plasticity. There were practically no debris and observable cracks along the scratch marks. It could be suggested that the same approach could be usefully employed to study the surface and through the thickness mechanical properties of various graded bioactive and composite coatings.

Acknowledgement

The authors wish to acknowledge the financial support from the Research Committee of The Hong Kong Polytechnic University (Project code: G-YX34) and Ministry of Science and Technology Republic of Serbia (through the projects of Fundamental research and EUREKA E! 3033 Bionanocomposit). This work was presented at the Workshop of EUREKA Project E! 3033, which was held in Bucharest and Sinaia, Romania, January 2006.

References

[1] D. R. Bloyer, J. M. Gomez-Vega, E. Saiz, J. M. McNaney, R. M. Cannon, A. P. Tomsia, Acta Mater. **47**, 4221 (1999).
[2] J. M. Gomez-Vega, E. Saiz, A. P. Tomsia, J. Biomed. Mater. Res. **46**, 549 (1999).
[3] T. Oku, K. Suganuma, L. R. Wallenberg, A. P. Tomsia, J. M. Gomez-Vega, E. Saiz, J. Mater. Sci.: Mater. Med. **12**, 413 (2001).
[4] J. M. Gomez-Vega, E. Saiz, A. P. Tomsia, T. Oku, K. Suganuma, G. W. Marshall, S. J. Marshall, Adv. Mater. **12**, 894 (2000).
[5] R. Roop Kumar, M. Wang, Mater. Sci. Eng. **A338**, 230 (2002).
[6] C. Y. Tang, P. S. Uskokovic, C. P. Tsui, K. C. Chan, Samuel C. L. Lo, X. L. Xie, Mater. Sci. Forum **494**, 469 (2005).
[7] J. Lintymer, N. Martin, J. -M. Chappe, P. Delobelle, J. Takadoum, Surf. Coat. Technol. **200**, 269 (2005).
[8] S. Chowdhury, E. de Barra, M. T. Laugier, Surf. Coat. Technol. **193**, 200 (2005).
[9] V. Nelea, C. Morosanu, M. Iliescu, I. N. Mihailescu, Surf. Coat. Technol. **173**, 315 (2003).
[10] V. Nelea, H. Pelletier, P. Mille, D. Muller, Thin Solid Films **453-454**, 208 (2004).
[11] Q. Wang, S. Ge, D. Zhang, Wear **259**, 952 (2005).
[12] C. Y. Ning, Y. J. Wang, X. F. Chen, N. R. Zhao, J. D. Ye, G. Wu, Surf. Coat. Technol. **200**, 2403 (2005).
[13] W. C. Oliver, G. M. Pharr, J. Mater. Res. **7**, 1564 (1992).
[14] J. M. Gomez-Vega, E. Saiz, A. P. Tomsia, G. W. Marshall, S. J. Marshall, Biomaterials **21**, 105 (2000).
[15] R. Teghil, L. D'Allesio, D. Ferro, S. M. Barinov, J. Mater. Sci. Lett. **21**, 379 (2002).
[16] F. C. Barbieri, C. Otani, C. M. Lepienski, W. I. Urruchi, H. S. Maciel, G. Petraconi, Vacuum **67**, 457 (2002).
[17] A. Toth, M. Mohai, T. Ujvari, T. Bell, H. Dong, I. Bertoti, Surf. Coat. Technol. **186**, 248 (2004).
[18] Y. Wang, T. Lei, B. Jiang, L. Guo, Appl. Surf. Sci. **233**, 258 (2004).
[19] W. Lu, K. Komvopoulos, J. Tribol. ASME **123**, 717 (2001).

*Corresponding author: nht@elab.tmf.bg.ac.yu